Additive Manufacturing Letters 9 (2024) 100196

Contents lists available at ScienceDirect

Additive Manufacturing Letters

journal homepage: www.elsevier.com/locate/addlet

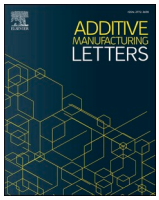

Short Communication

Measurement of focal plane error in laser powder bed fusion machines

Jaime Berez [a,*], Enea Dushaj [b], Elliott Jost [b], Christopher Saldaña [b], Katherine Fu [c]

[a] Center for Precision Metrology, The University of North Carolina at Charlotte, 9201 University City Blvd, Charlotte, NC 28223, USA
[b] George W. Woodruff School of Mechanical Engineering, Georgia Institute of Technology, 801 Ferst Dr. NW, Atlanta, GA 30332, USA
[c] Department of Mechanical Engineering, University of Wisconsin-Madison, 1513 University Ave., Madison, WI 53706, USA

A B S T R A C T

Amongst the many sub-systems that make up laser powder bed fusion (PBF-LB) machines, the optomechanical sub-system stands out due to its potential for off-nominal performance but incommensurate level of study on performance evaluation. Nominally, the optomechanical system focuses the laser onto a planar field which is at a controlled position and orientation relative to the powder bed. Deviations from this assumed condition, sometimes referred to as defocus or focus offset, have the potential to significantly impact the manufacturing process by influencing the energy intensity at the process zone. Herein, a novel, high-throughput, low-cost, artifact-based methodology to measure focus offset is detailed. In a single continuous build process, tracks at varying offsets from the build plane were created by ablating the coating on discrete coupons located throughout the build area. By examining these track widths, the focus offset was determined at a relatively fine spatial resolution over the build space, down to 25 mm intervals along the *x* and *y* directions, thus ascertaining the discrepancy between the laser focal plane and the build plane, i.e., focal plane error. Results were found to agree with reference measurements to within 0.27 mm over the entire build space and defocus levels ranging from approximately -1.6 to 1.7 mm were discovered. Field sag and optomechanical misalignment were the major casual factors. It is concluded that similar or more severe levels of defocus may be present in the typical PBF-LB machine, which may impart considerable impacts to the overall PBF-LB process.

1. Introduction

Laser powder bed fusion (PBF-LB) is a prevalent form of metal additive manufacturing (AM) with relatively high commercial adoption in the aerospace and medical sectors, amongst others. These applications naturally require a high degree of process control, which is a driving force behind the emphasis on research and development in material and component qualification [1]. Good process control also necessitates examination of the operation principles and performance of the AM machines themselves [2]. As a broad overview, PBF-LB machines utilize a laser(s) to fuse a feedstock powder which is spread over a powder bed in thin layers by a powder spreading device, e.g., a recoater. Solid-state Nd:YAG or Yb-fiber single-mode Gaussian lasers are used in the vast majority of commercially available PBF-LBF systems [3]. Commercial machines commonly utilize galvanometer driven mirrors to steer the laser beam through an F-theta scan lens which focuses the beam onto a nominally planar working field [4]. The laser beam undergoes a converging-diverging behavior, i.e. beam caustic, with the point of focus, i.e., beam waist, being where the spot size is at a minimum along the beam axis. Given this understanding, one major performance characteristic to consider is the offset between the focus point of the beam and the powder bed, sometimes referred to as "defocus," "focus shift," or "focus offset" in literature pertaining to AM [5–9]. Focus offset can be introduced intentionally, but it also may be inherent in the performance a PBF-LB machine [8] that displays off-nominal characteristics due to factors such as imperfect optical elements, machine construction quality, set-up or calibration errors, thermal/environmental factors, and performance drift. As of yet, there has been very little study of either potential focus offset errors or suitable measurement methods for capturing them – the few examples there are will be reviewed in the ensuing paragraphs.

The motivation to study laser defocus in PBF-LB systems is clear if one considers that defocus leads to fundamental changes in energy input to the process zone. Prior work has shown that a defocused beam in the PBF-LB process can produce lowered beam energy intensity and changes in welding mode, leading to decreases in melt pool depth [5–7,10–12], microstructural coarsening [6,7], variations in porosity formation [13,14], and improved surface texture [13,14]. Liu et al. [12] were able to replicate experimentally observed changes in melt pool geometry and welding mode via CFD simulations. Various results [5,7,10] also indicated that negative defocus, i.e., with the beam waist below the substrate, produced deeper melt pools than equivalent levels of positive defocus, attributed to the converging beam increasing laser absorptivity and beam reflections inside the melt pool depression. Other results [12] have stood in contrast to these findings, though. In summary, these studies suggest that a focus offset of merely ±2-3 mm, if not less, is

* Corresponding author.
E-mail address: j.berez@charlotte.edu (J. Berez).

https://doi.org/10.1016/j.addlet.2024.100196
Received 30 November 2023; Received in revised form 17 January 2024; Accepted 23 January 2024
Available online 28 January 2024

capable of imparting significant impacts to melt pool depth and welding mode.

The present work is motivated by these findings but asks the question: how can focus offset be measured? Of those studies reviewed above, only minimal detail was provided in regard to this. One study [12] appeared to use a commercial camera-based beam profiling instrument (this was implied but details were not provided) and another [11] briefly discussed the use of a CCD-detector for beam profiling. In all other cases [5–7,13,14], it appears that authors simply assumed perfect calibration by the machine OEM, i.e., zero offset at $z = 0$ in the build coordinates. As the present work will demonstrate, this may be a poor assumption as significant focus offsets are likely inherent in PBF-LB machines and not constant across the build area. In fact, in several cases [6,10–12], authors have even commented on potential measurement errors in determining the true beam waist location. Altogether, while there is reason to think that focus offset may have serious impacts on the PBF-LB process, the conclusions of prior studies and the potential scope of the impacts should be viewed with some skepticism without a rigorous examination of the methods used to measure beam focus on-machine.

Generally speaking, in the field of laser optics, beam focus is measured via the laser beam caustic which is established by gathering spot size measurements along the axis of the beam. Several existing commercial instruments, sometimes called beam profilers, are capable of such measurements and can be broadly categorized as camera-based and diffraction-based instruments. Utilizing either for beam caustic measurement on a PBF-LB machine is challenged by the significant cost of the instrument, time required to complete a caustic measurement, and potential prerequisite access to PBF-LB machine non-standard controls – all this possibly explaining the scarce use of these instruments in the peer-reviewed literature. Notably, these instruments are not conducive to measurement of the beam caustic over the entire build area due to instrument size, laborious set-up for each position in the build space, and the inability to measure a beam with a nonzero incidence angle, i.e., at nonzero (x, y) positions. Although some diffraction-based instruments [15] are capable of nonzero incidence angle beam measurement, instrument size is still a limiting factor in these cases.

Some novel focus measurement methods for PBF-LB applications have been proposed to complement beam profiling instruments. That said, these novel methods, which include a pin-hole diffraction technique [16] and variations on monitoring radiation emitted from the process zone [17–19], do not appear to have gained traction due to their experimental complexity, poor scalability over the build area, and lack of verification. Notably, the authors are not aware of any published results concerning focus characterization over the build space as a function of (x, y), possibly due to deficiencies in the currently available methods.

Many a skeptical user of a PBF-LB machine has wondered: Is the laser beam focus realized as theoretically intended? The review of prior work presented here suggests this is a worthwhile question, but one lacking the appropriate supporting method to measure the variable in question. Notably, PBF-LB machine builders do not currently assuage these concerns – it is fair to say that their methods used to evaluate focal error, if any, are generally not formally communicated to customers nor are machines delivered with statements of performance. Critically, the ability for the user to measure laser focal offset (1) on-machine, (2) over the entire build space, and (3) with relative ease and affordability are desired in an ideal measurement method. These abilities would allow performance limitations of machines to be evaluated, manufacturer specifications to be verified, error sources to be identified, and overall machine down-time and maintenance cost minimized. In response to these gaps, this manuscript makes a preliminary contribution to the development of a novel method for determining focal plane error, i.e., the discrepancy between the focal plane and build plane, that is rigorous and widely applicable

2. Materials and methods

2.1. PBF-LB optomechanical system

Measurements of laser focus over the build space of a commercial EOS M280 PBF-LB machine were performed. This PBF-LB system utilizes a single-mode Gaussian 400 W Yb-fiber laser (wavelength $\lambda = 1064$ nm) to selectively fuse material over a 250 × 250 mm build space (x and y dimensions). Fig. 1(a) shows a graphical description of the system, with important characteristics noted. A brief description of the optomechanical system is provided here. A columnated laser is directed via a fiber optic to a beam expander, which defines the beam entrance diameter, d_{ent}, to the subsequent scan system. The beam is steered by two galvanometer driven mirrors through an F-theta scan lens and a cover lens. The F-theta optic focuses the beam onto a nominally flat focal plane and has a focal length reported as $f = 410$ mm by the AM machine builder. No other specifications of the optical element were reported by the AM machine builder and none were available in any available product literature of the lens manufacturer nor in the peer-reviewed body of work. Nominally, the PBF-LB system is intended to focus the laser beam onto a *focal plane*, which exists in relation to a *build plane*, abstractly depicted in Fig. 1(b). *Focal plane error* is then the difference between the focal plane and the the build plane. For lack of standard terminology in the literature or industrial standards, these terms are briefly defined below.[1]

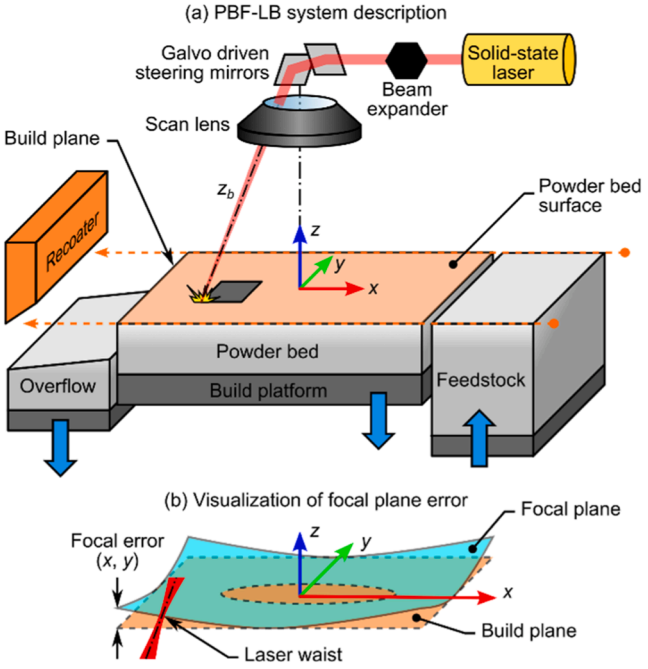

Fig. 1. (a) PBF-LB system description, with critical optomechanical components noted. (b) Visualization of focal plane error. Not to scale.

[1] It should be noted that ISO/ASTM 52900:2021, ISO/ASTM 52930:2021, and ISO/ASTM 52941:2020 set out terms such as "build surface," "working plane," and "focus point" but for lack of context-specific definitions, these terms are not used here.

Build plane: An ideal geometrical element associated with the powder bed surface as established by a powder spreading device,[2] establishing $z = 0$.[3]
Focal plane: A surface, over which the laser beam is in focus, i.e., where the spot size is at a minimum.
Focal plane error: The focal plane in relation to the build plane, valued in the z direction and defined as a function of build coordinates x and y, where $z = 0$ is defined by the build plane.

The phenomena of beam focus at any (x, y) position is captured by the concept of a beam caustic, which expresses the beam spot size as a function of position along the beam travel direction, z_b. Fig. 2 shows the beam caustic for the assessed PBF-LB system, calculated using the formulae below. Eq. (1) defines the focused beam spot size, i.e., beam waist diameter, d_0. Here, d_{ent} is the beam entrance diameter and M^2 is the beam quality factor, where $M^2 = 1.0$ indicates ideal divergence behavior for a Gaussian beam. Eq. (2) defines the Rayleigh length of the beam, z_R, indicating the distance over which the beam spot size doubles in area. Finally, Eq. (3) defines the beam spot size, d, as a function of z_b, i.e., the beam caustic. Note that there exist numerous methods for expressing the spot size of Gaussian beams – here, d_0 and all other references to spot size correspond to the $D4\sigma$ definition, which is 4 times the standard deviation, σ, of the beam intensity distribution, i.e., $\pm 2\sigma$. For the assessed PBF-LB system, M^2 is taken as 1.0 and d_{ent} as 7.5 mm, based on measurements conducted by the authors on a highly similar EOS M290 PBF-LB system which indicated that M^2 was very close to 1.0 (measured to be 1.05) and d_0 was 74 μm (used to back-calculate d_{ent}). For reference, the Rayleigh length for the studied PBF-LB system was calculated to be $z_R = 4.04$ mm.

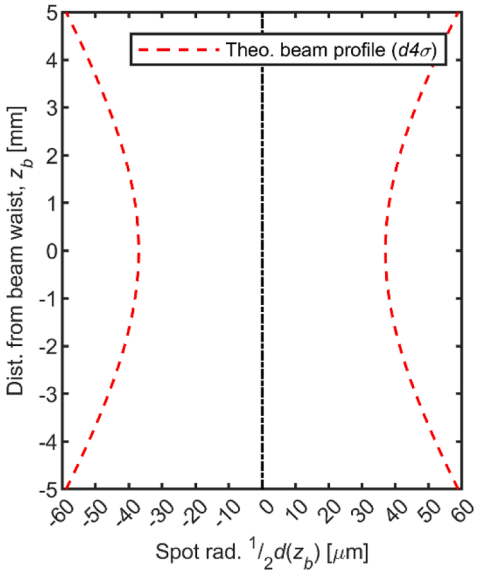

Fig. 2. Theoretical beam caustic.

$$d_0 = 2\omega_0 = \frac{4M^2\lambda f}{\pi d_{ent}} \tag{1}$$

$$z_R = \frac{\pi d_0^2}{4M^2\lambda} \tag{2}$$

$$d(z_b) = d_0\sqrt{1 + \left(\frac{z_b}{z_R}\right)^2} \tag{3}$$

2.2. Laser focal plane measurement method

This work employs a novel artifact-based method of beam caustic measurement. The PBF-LB system laser was used to ablate the anodized coating on aluminum coupons in a controlled manner. To demonstrate the principle, consider a single coupon positioned at (x, y) = (0, 0). Ablated tracks were formed by single laser scan paths over the coupon. Tracks were ablated at various offsets between the coupon top surface and the known build plane position, $z = 0$. As the width of these tracks are expected to approximately reflect the beam spot size at each z position, these widths represent a proxy of the beam caustic and can be used to determine the laser focus offset at any (x, y) position in the PBF-LB machine coordinate system. This approach can be replicated at many (x, y) positions, at a desired level of granularity, thereby determining focal plane error.

Coupons were polished 6061-T6 aluminum, 6.35±0.05 mm thick, 19 × 19 mm in their footprint, and anodized (type II) black as per MIL-A-8625. Coupons were positioned over the 250 × 250 mm build space using a fixture that allowed coupons to be arrayed in a gridded pattern at known (x, y) positions in 25 mm intervals. Fig. 3 shows the laser scan paths applied to the coupon located at (x, y) = (0, 0), represented in the static build coordinate system. Each track was ablated at a distinct z offset relative to the build plane ranging between -5.0 to -5.0 mm. These z values were chosen to range across approximately $\pm 1 z_R$ of $z = 0$. Tracks were 4.0 mm long.

Fig. 4 shows (a) the PBF-LB system and (b) the coupon positioning fixture with coupons placed on some, but not all possible locations. Fig. 4(c) shows a simplified schematic of coupons laid out at 25 mm intervals in the x and y directions. While the track patterns are not drawn to scale for legibility, note that, depending on the coupon (x, y) location, the pattern is rotated such that the tracks are oriented in the radial direction. This was done to ensure that track width was not influenced by beam incidence angle. A to-scale coupon and track pattern is also shown on the right of (c). As can be seen in Fig. 4(a), gas flow was in the -y direction. No effect of gas flow on laser focus is suspected and only very minor levels of vapor formation, which were easily evacuated by gas flow, were observed during ablation. It should be noted that vapor

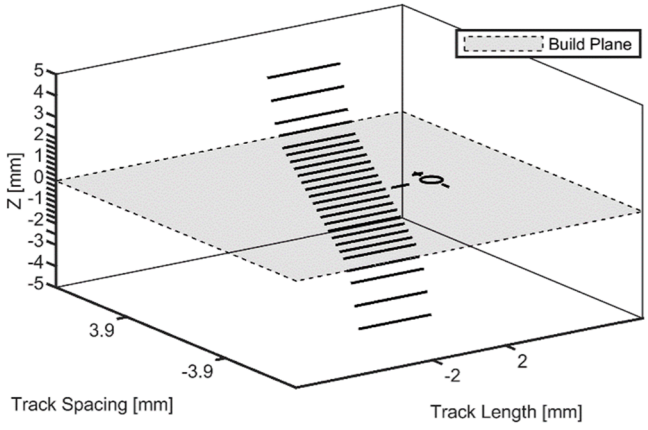

Fig. 3. To-scale 3D visualization of programmed laser scan paths for the coupon located at (x, y) = (0, 0). The z axis corresponds to the build direction.

[2] In the examined PBF-LB machine, the powder bed is formed by a recoating mechanism that with a straight edge aligned in the y direction which is translated in the -x direction over a straight path, seen in Fig. 1(a). Recoating mechanisms vary in commercial implementations.

[3] The build plane, a theoretically perfect plane, models the surface of the powder bed, a nominally planar feature with non-zero form error. The form error of the powder bed, and any potential error in establishing the build plane as a reference feature, is considered negligible in the context of this work.

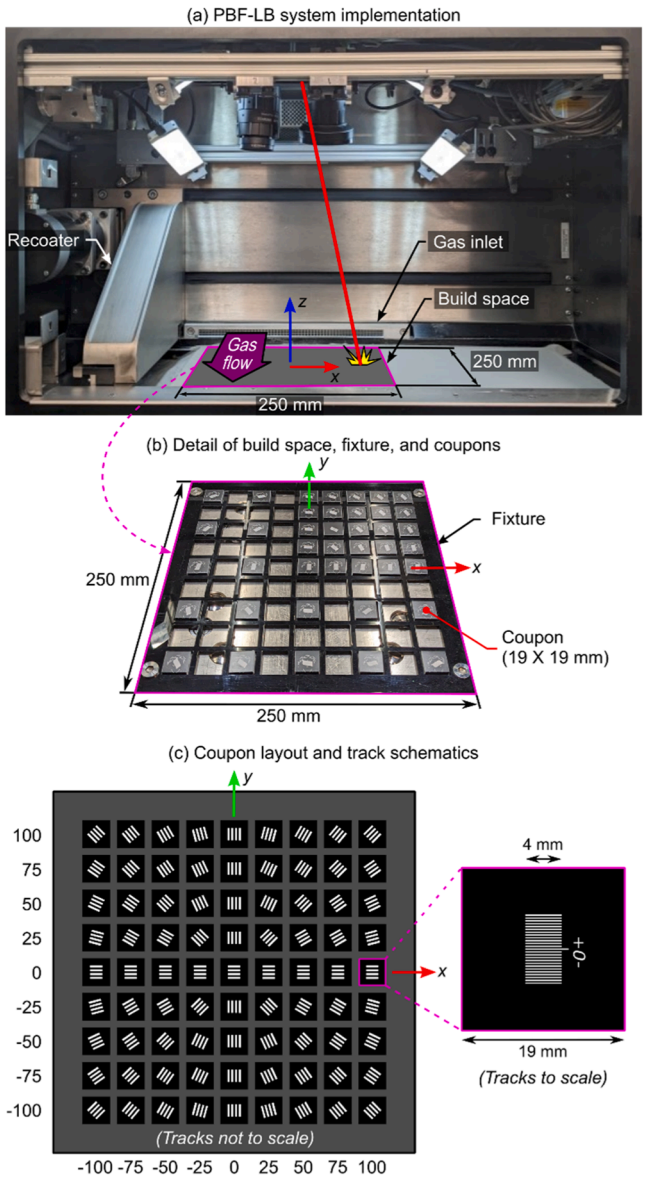

Fig. 4. (a) PBF-LB system build chamber. (b). Coupon positioning fixture. (c) Visualization of track directions as a function of build area location. Tracks are not to scale and only 4 are shown for legibility. An individual coupon with 25 tracks to scale is shown on the right.

clouds may play a role in attenuating laser energy during a normal building process, but this concept is out of the scope of the present study.

To conduct a measurement of a beam caustic using a coupon, the following procedures were followed. (1) The build platform was made parallel to and coincident with the build plane. This involves adjusting a kinematic leveling system for the build platform to achieve parallelism to a reference surface on the recoater, verified by measurement with a dial indicator and feeler gages. The physical surface of the build platform was measured to be parallel to and coincident with the build plane to within 50–100 μm after this procedure. (2) Material coupons were placed at desired locations on the build platform. (3) The build platform z position was adjusted to compensate for the thickness of the material coupons and additionally incremented upwards by 5.00 mm. As such, 'building', i.e., laser ablation of the coupons, would begin with the top of the material coupons located at $z = 5.00$ mm. As a final preparation step, the scan lens optic was cleaned with a lint-free optical grade wipe wetted with high-purity isopropyl alcohol. (4) A build file, containing the tracks at all z positions for all coupons was executed.

All tracks were ablated using a laser power of $P = 150$ W and laser speed of $V = 2000$ mm/s. During a 'build,' the PBF-LB machine automatically increments the build platform in the -z direction, pausing for a 'layer' to expose coupons to the laser as defined by the build file. This approach meant that an extremely large number of material coupons representing many (x, y) coordinates could be processed in a single build sequence lasting approximately 15–30 min, including build start/stop procedures.

A Leica DVM6 Digital Microscope was used to obtain a monochromatic image of each 4 mm ablated track approximately at the center of the track. A mid-magnification objective lens with a total feild-of-view of 12.55 mm was used with a magnification of 500x. The pixel side length for each image is 0.168 μm. Each track image was binarized using Otsu's method. The boundaries of the track in the binarized image were determined. An orthogonal least squares fit was applied to each edge of the track using the (x, y) coordinates of the corresponding pixels. At each pixel along one edge, the point on the opposing edge that creates a line segment with a slope orthogonal to the centerline was used to make one width measurement. Each width measurement in pixels was then converted to a physical length measurement. Approximately 3000 width measurements were made for each track. A mean and standard deviation for the width of each track was calculated. This process was repeated for each etched track on each coupon.

3. Results

3.1. Measurement of a typical coupon

Fig. 5 shows the process by which track width measurements were made. Tracks from a coupon located at (x, y) = (0, 0) are used as an example. Due to the irregularity of the track edges, width measurements vary over the length of the track. Fig. 5 shows an example of width measurement, with ever 50th point of width measurement noted as a green dashed line. Widths values were approximately normally distributed as shown in Fig. 5(d), with a typical standard deviation on the order of 3 μm.

Fig. 6 shows track width measurements from a single coupon. Track width shows a trend reflecting the converging-diverging behavior of the laser beam, with a minimum contained within the z domain investigated. Error bars describe the variation in width displayed by each track as ±1σ. These values are well above the resolved pixel size of the micrographs acquired, indicating that natural process variation is likely the major contributor to variability, not the measurement method. As first-principles describe a hyperbolic trend in spot diameter as a function of z_b, seen in Eq. (3), a hyperbolic fit was applied to the average track width, w_b, as a function of the offset from the build plane, z, for each coupon. Fitting was performed via a Nelder-Mead simplex algorithm [20]. The fitted hyperbola models the empirical data well, as seen via the solid blue curve in Fig. 6. For reference, the theoretical beam caustic, earlier presented in Fig. 2, is also provided in dashed red. It has been shifted in z by 0.75 mm, to account for the focus offset apparent in the experimentally measured beam caustic. There is fair agreement between the fit and theoretical hyperbolas, with only a 7 μm difference between the vertex values but a slightly steeper slope towards the extents of studied z range. This may be explained by the decrease in energy intensity of the spot that comes with beam defocus, leading to ablation scaling less directly with theoretical spot size further away from the beam waist. Further examination of the theoretical relationship between ablated track width and spot size is warranted, but out of the scope of the present work. The z value of the minima of the hyperbolic fit was considered the focus offset for the (x, y) position of a given coupon.

3.2. Focal plane determination – flatness, parallelism, and position

Two independent experiments were conducted to measure focal plane error in the examined PBF-LB machine. The first was intended to

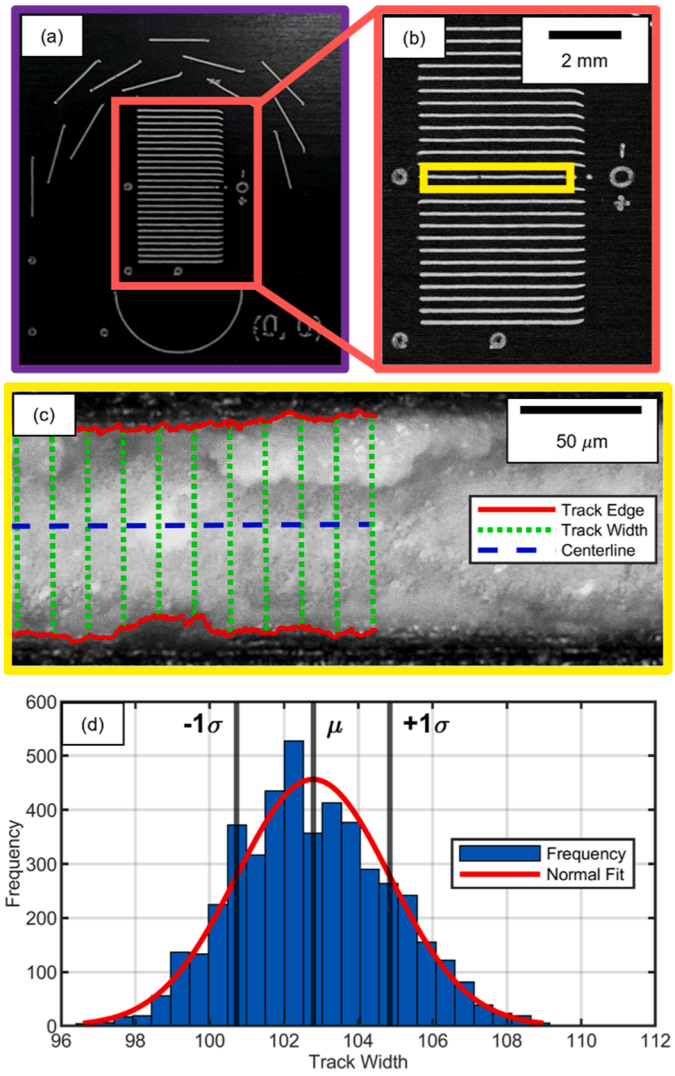

Fig. 5. Visualization of workflow for ablated track width measurement. (a) Single coupon originating from (x, y) = (0, 0). This coupon includes tracks not examined in this study. (b) Detail of tracks ablated at varying z heights. (c) Detail of a single ablated track showing a portion of the determined edges, centerline, and every 50th width measurement. (d) Distribution of width measurements along a single track.

assess any inherent errors present when following all best practices in build setup. In other words, the build platform was made parallel with and coincident to the build plane (as defined by the recoater), as was described in Section 1.2. As such, this first experiment assessed focal plane error for the PBF-LB machine in a state as delivered by the machine manufacturer and including all performance impacts suffered since in operation. In this experiment the machine was representative of an in-service condition. The second experiment was intended to enable comparison between the focal plane measurement method and an arbitrary but independently measurable tilt (rotation about the x and y axes) introduced to the build platform. In other words, given an initial state (experiment #1) and a final state (experiment #2) with a known disturbance, i.e., the build platform tilt, applied between the two, the aim was to assess if this disturbance could be accurately measured.

For experiment #1, the procedures detailed in Section 1.2 were followed to produce 41 coupons over the build space. Coupons were positioned at 25 mm intervals in the $+x/+y$ quadrant and 50 mm intervals elsewhere to provide a relatively high density of measurements while balancing experimental effort, under the assumption that errors would show mirror symmetry about the x and y axes. After processing all

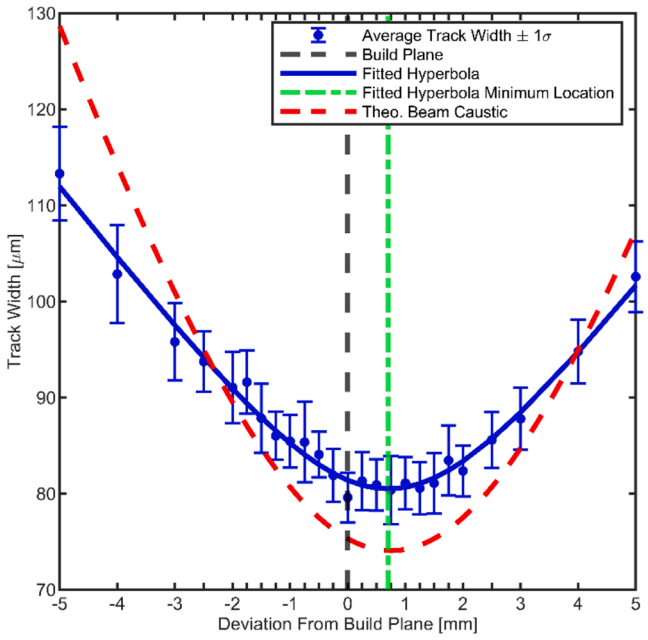

Fig. 6. Typical track width measurements, caustic fitting, and minima extraction for focal point error. Note that the theoretical caustic is shifted in z by 0.75 mm.

coupons as detailed in Section 2.1, the focal plane error was determined and is displayed in Fig. 7. Focus offset values are plotted over the nominal (x, y) locations of each coupon track pattern. The measured focal plane error ranges from -1.60 mm to 1.17 mm. Note that the method employed enabled measurements of focal plane error to within 25 mm of the boundaries of the 250 × 250 mm build space, indicated by the black dashed line in subsequent figures. As is evident, the focal plane exhibited what may be considered form or flatness error, more commonly termed field sag in optical literature [4]. The total variation of focal plane error at the measured points was 2.77 mm. Investigation of focal plane error even nearer to the build space bounds would have likely revealed increasing error. As can be seen in (b), a plane was fitted to the data via least-squares routine to minimize deviations in z. This fitted plane exhibited parallelism of 0.37 mm relative to the build plane. Parallelism, here, was evaluated as the difference between the maximum and minimum distance between the fitted focal plane (the feature) and the build plane (the datum), over the area measured, similar to the practice of determining parallelism in coordinate metrology contexts.

In experiment #2, the build platform leveling mechanism was used to introduce an arbitrary but independently measurable tilt about the x and y axes – 1.67 mm of parallelism error to the build plane. This also simulated the characteristics of a machine with some form of opto-mechanical misalignment. Dial gauge indicator measurements were used to obtain parallelism measurements between the recoater and build platform, i.e., the change in the build platform orientation between experiment #1 and #2. The 'build' was then conducted with laser ablation of 25 coupons over the build space, arranged to investigate the focal plane at 50 mm intervals. After processing all coupons as detailed in Section 2.1, the focal plane error was determined, displayed in Fig. 8. The measured focal plane error ranged from -1.22 to 1.71 mm. The total variation of focal plane error over the measured points was 2.93 mm. As can be seen in (b), a plane was fitted to the data via least-squares routine to minimize deviations in z. This plane exhibited parallelism of 1.63 mm relative to the build plane.

As alluded to prior, it is possible to partially verify the accuracy of the measurement method through a comparison of the presented measurements to a known quantity. Although the state of the focal plane in experiment #1 is not known via an independently verifiable method, a

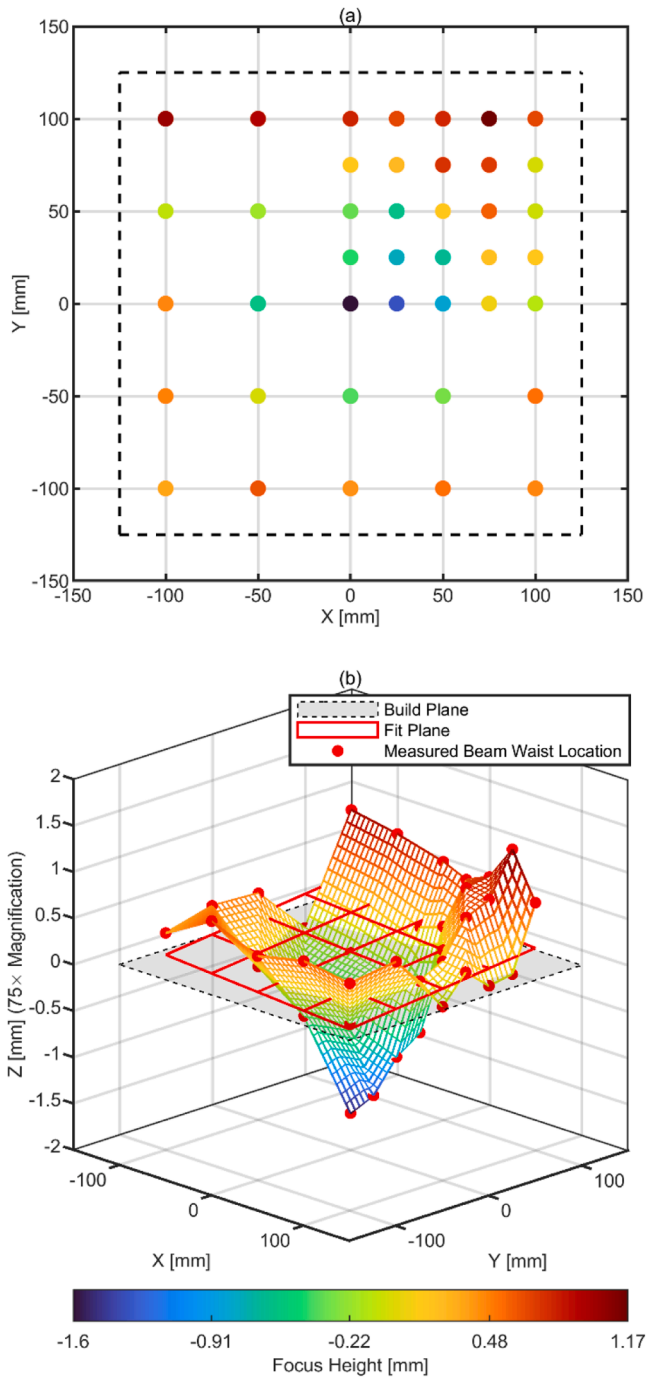

Fig. 7. (a) Focal plane error measurements over the build space. (b) 3D visualization of the focal plane error.

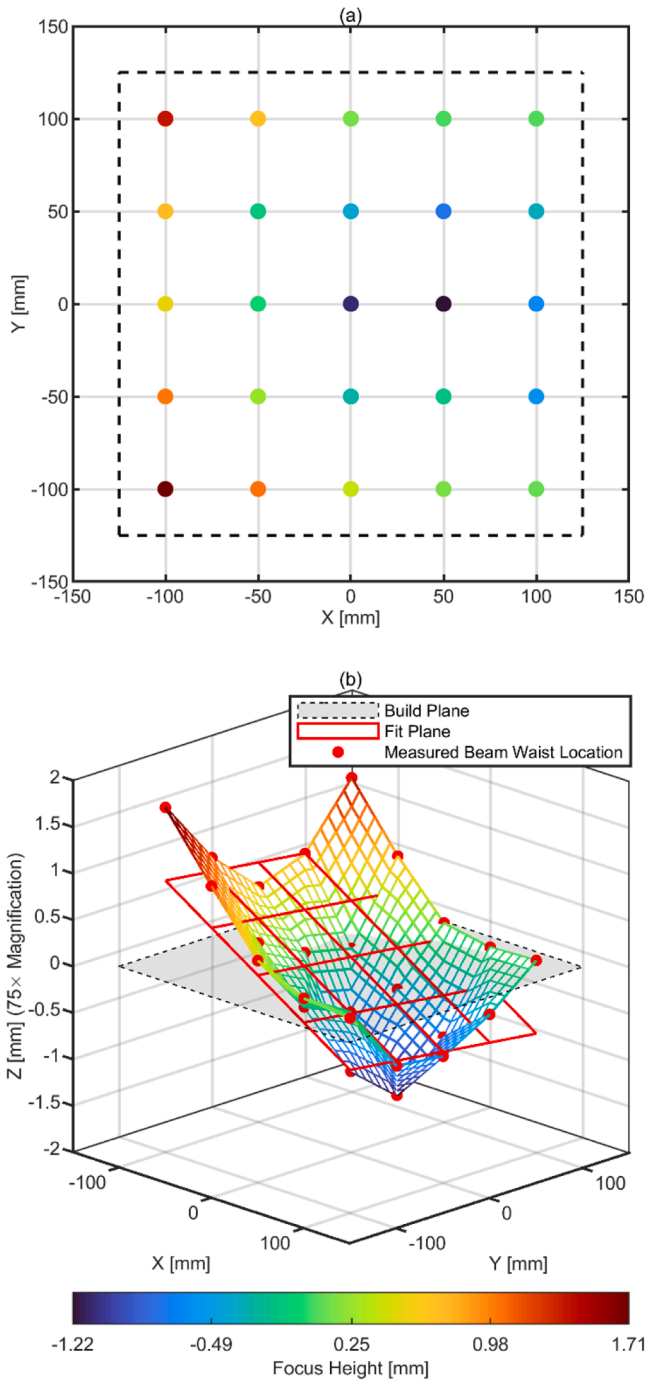

Fig. 8. (a) Focal plane error measurements over the build space. (b) 3D visualization of the focal plane error.

known change was introduced and the initial and final states were captured by experiments #1 and #2, respectively. Consider that prior to experiment #1, the build platform was made parallel and coincident to the build plane over the build space, as was detailed in Section 1.2. Now consider that prior to experiment #2, the build platform was intentionally tilted and this was measured via a dial indicator, measuring the displacement of the build platform at each location where a coupon was to be ablated. This produced an array of reference values over the (x, y) domain of the build space. The results of experiment #2, nulled by experiment #1, should then ideally match the reference measurement. Fig. 9 presents this concept quantitatively. The red points represent the focal plane error measurements of experiment #2 minus those of experiment #1. The red plane was then fitted to this data. The blue plane represents the known tilt introduced between these two measurements, as measured via the dial indicator. The fit plane and the reference measurements show good agreement, with differences only ranging from 0 to -0.27 mm over the measured build area.

4. Discussion

The measurements of focal plane error performed provide novel insight into the performance of a typical PBF-LB commercial system. Considering the results of experiment #1, the focal plane is bowl-shaped with a low point at $(x, y) = (0, 0)$ and approximate radial symmetry

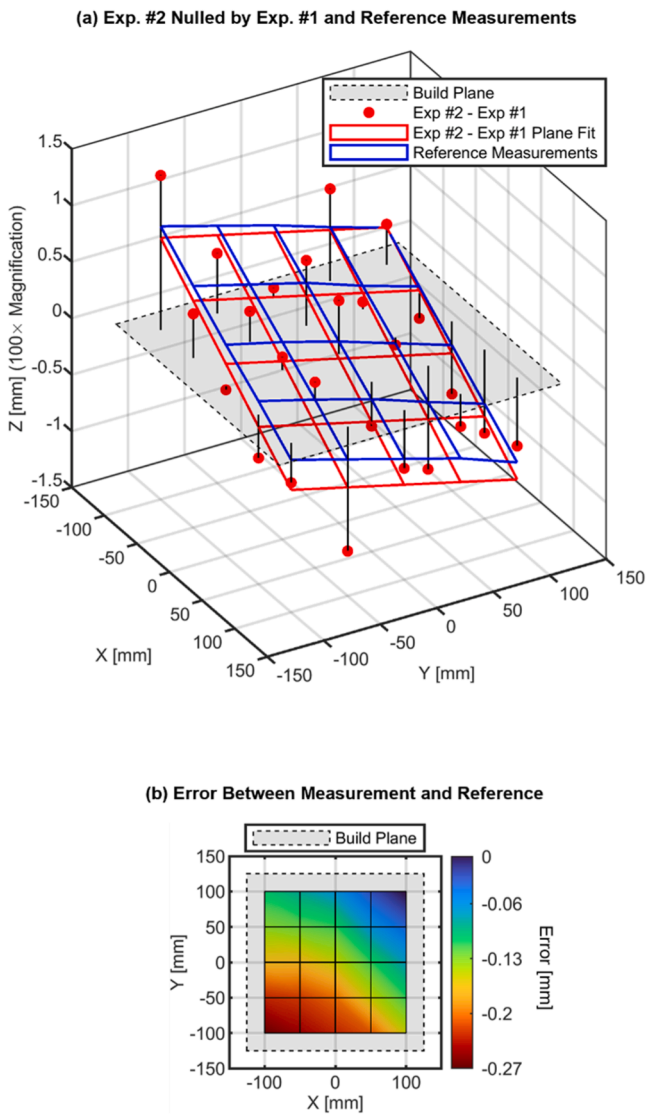

Fig. 9. (a) In red: The measured focal plane of experiment #1 subtracted from the measured focal plane of experiment #2. In blue: The reference measurements of the build platform tilt introduced between experiments #1 and #2. (b) The error between the difference of experiments #1 and #2 relative to the reference plane.

about the origin, to be expected in systems with typical F-theta optics [4,21]. The non-flat focal plane, combined with the construction imprecision of the PBF-LB machine, i.e., actual distance between the optic and recoater-edge, has led to the lowest point of the focal plane being approximately -1.6 mm at the origin and up to 1.17 mm above towards the build space limits. The focal plane was quite parallel to the build plane; the plane fit to the focal surface displayed 0.37 mm parallelism to the build plane. The results of experiment #1 also show that, in this particular PBF-LB machine, both negative and positive defocus can be present, and this may have corresponding impacts on the process.

The results of experiment #2 show that the measurement method can capture various forms of optomechanical misalignment. Poor optical element installation could result in a focal plane with poor parallelism relative to the build plane. Conversely, poor recoater system setup (such as incorrect blade installation) or mechanical disturbances and wear in the assembly (such as from recoater crashes) could produce the same net result. Experiment #2 simulated such a scenario, capturing a focal plane with parallelism to the build plane of 1.63 mm. Overall, it is difficult to say how the proposed methodology compares to other approaches and whether or not similar error sources (field sag, optomechanical misalignment) have been discovered in varying PBF-LB systems – the literature is extremely sparse in addressing these questions and further work from the AM research community is warranted.

The results of this work suggest a reexamination of laser focus offset as a process parameter. As was presented in earlier, prior work has found significant changes in the PBF-LB process over focus offsets similar in magnitude to those found in this work, even if conclusions from these results should be tempered by the lack of an appropriate concurrent focus offset measurement method. The results of this work also factor into significant efforts that have been recently aimed at understanding variable microstructure, defect content, and mechanical properties observed over the build space. Various authors [22,23] have speculated on the impact of a variety of candidate process issues including shielding gas flow, spatter, laser attenuation by condensate clouds, and variable laser spot size, shape, intensity, and incident angle. The novel measurement presented herein is an important and enabling tool which can now be aimed at understanding the contributions of focal plane error to this larger problem.

It should be noted that the measurement approach does not directly account for spot shape distortion due to potential telecentricity. Nonetheless, since the minima of the beam caustic for each (x, y) location was used to determine focus offset, this should not have impacted the results. Further investigation into this aspect is nonetheless warranted, and the measurement method developed herein could be reapplied to understand this dimension of the problem.

5. Conclusion

The novel method for focal plane error measurement presented here plainly has several advantages over existing methods. With relatively minor experimental effort and expense, focal plane error was measured over nearly the entire build space at a fine level of granularity, up to 25 mm increments in x and y. The novel approach only required inexpensive and commonly available coupon material, a simple fixture, and one build file to be executed by the PBF-LB system. While the subsequent microscopy measurements are currently labor intensive and require custom software to process, these aspects of the process are amenable to automation. While optical system manufacturers certainly are capable of simulating and verifying characteristics like field sag at a high spatial density with low uncertainty, these principles are limited in their application to PBF-LB machines, where on-machine performance testing is critical to capturing the state of the machine as a function of many factors.

Overall, this method enabled a focal plane error measurement not yet realized in the peer-reviewed literature familiar to the authors. Critically, components of focal error (focal plane form, plane parallelism, and plane position) corresponding error sources (field sag, optomechanical alignment) can be identified, which would enable meaningful diagnosis and/or corrective action by users. The results also revealed that typical focus offsets in PBF-LB machines, which may be on the order of 2-3 mm over the build space, are significant in terms of process impacts – further investigation is warranted. Do certain levels of focal error correlate to melt pool geometry variations and other process perturbations? How much can this vary over the build area?

The apparent simplicity of the measurement method should not imply that further development and study are unnecessary. Future work should focus on three areas: Systematic determination of optimal process parameters for ablation, development of an analytical model which relates ablated track width directly to beam spot size, and validation against a reference measurement of the beam caustic. Optimal process parameters may be determined through ablation process mapping, an analytical model could be developed to explain discrepancies between ablated track width and actual spot size, and validation will be key to establishing measurement uncertainty. Through progress in these areas, the measurement method can be employed with lowered uncertainty,

increased confidence, and improved process insight.

CRediT authorship contribution statement

Jaime Berez: Conceptualization, Methodology, Writing – original draft, Supervision. **Enea Dushaj:** Investigation, Formal analysis, Writing – original draft. **Elliott Jost:** Conceptualization, Methodology, Writing – review & editing. **Christopher Saldaña:** Funding acquisition, Supervision, Writing – review & editing. **Katherine Fu:** Funding acquisition, Supervision, Writing – review & editing.

Declaration of competing interest

The authors declare the following financial interests/personal relationships which may be considered as potential competing interests:

U.S. Patent Application No. 63/472,124 has been filed by the authors. It contains information related to the work presented in this manuscript.

Data availability

Data will be made available on request.

Acknowledgments

The authors acknowledge J. Weaver, D. Deisenroth, and S. Moylan, of the Production Systems Group of the Intelligent Systems Division at the National Institute of Standards and Technology, for their informal conversations and feedback on this work. A. Argondizzo and K. Branigan of Coherent Inc. as well as A. Hedges of the II-VI/Coherent Foundation are similarly recognized. This work was supported in part by the U.S. Department of Energy [DE-EE0008303], the National Science Foundation [CMMI-1825640], and the II-VI/Coherent Foundation.

References

[1] M. Seifi, A. Salem, J. Beuth, O. Harrysson, J.J. Lewandowski, Overview of materials qualification needs for metal additive manufacturing, JOM 68 (2016) 747–764, https://doi.org/10.1007/s11837-015-1810-0.

[2] S. Moylan, J. Drescher, M.A. Donmez, Powder bed fusion machine performance testing, ASPE Spring Topical Meeting: Dimensional Accuracy and Surface Finish in Additive Manufacturing, Berkley, CA, 2014.

[3] I. Gibson, D. Rosen, B. Stucker, Powder bed fusion processes, I. Gibson, D. Rosen, B. Stucker (Eds.). Additive Manufacturing Technologies: 3D Printing, Rapid Prototyping, and Direct Digital Manufacturing, Springer, New York, NY, 2015, pp. 107–145, https://doi.org/10.1007/978-1-4939-2113-3_5.

[4] A. Argondizzo, K. Branigan, Advanced optics for laser additive manufacturing: f-Theta lenses for laser powder bed fusion, in: Proceedings of the Laser 3D Manufacturing X, SPIE, 2023, pp. 27–30, https://doi.org/10.1117/12.2650853. : pp.

[5] J. Metelkova, Y. Kinds, K. Kempen, C. de Formanoir, A. Witvrouw, B. Van Hooreweder, On the influence of laser defocusing in selective laser melting of 316L, Addit. Manuf. 23 (2018) 161–169, https://doi.org/10.1016/j.addma.2018.08.006.

[6] T.D. McLouth, G.E. Bean, D.B. Witkin, S.D. Sitzman, P.M. Adams, D.N. Patel, W. Park, J.M. Yang, R.J. Zaldivar, The effect of laser focus shift on microstructural variation of Inconel 718 produced by selective laser melting, Mater. Des. 149 (2018) 205–213, https://doi.org/10.1016/j.matdes.2018.04.019.

[7] X. Nie, Z. Chen, Y. Qi, H. Zhang, C. Zhang, Z. Xiao, H. Zhu, Effect of defocusing distance on laser powder bed fusion of high strength Al–Cu–Mg–Mn alloy, Virtual Phys. Prototyp. 15 (2020) 325–339, https://doi.org/10.1080/17452759.2020.1760895.

[8] J. Berez, E. Dushaj, Additive manufacturing machine tool qualification: methods and insights, in: Euspen, Leuven, BE, 2023 Joint Special Interest Group Meeting: Advancing Precision in Additive Manufacturing.

[9] J. Berez, E. Jost, E. Dushaj, C. Saldaña, Measurement of laser focal plane error in laser powder bed fusion systems, in: Knoxville, TN, 2022 ASPE-euspen 2022 Summer Topical Meeting: Advancing Precision in Additive Manufacturing.

[10] P. Liu, J. Hu, H. Li, S. Sun, Y. Zhang, Effect of heat treatment on microstructure, hardness and corrosion resistance of 7075 Al alloys fabricated by SLM, J. Manuf. Process. 60 (2020) 578–585, https://doi.org/10.1016/j.jmapro.2020.10.071.

[11] J.S. Weaver, J.C. Heigel, B.M. Lane, Laser spot size and scaling laws for laser beam additive manufacturing, J. Manuf. Process. 73 (2022) 26–39, https://doi.org/10.1016/j.jmapro.2021.10.053.

[12] B. Liu, G. Fang, L. Lei, W. Liu, Experimental and numerical exploration of defocusing in Laser Powder Bed Fusion (LPBF) as an effective processing parameter, Opt. Laser Technol. 149 (2022) 107846, https://doi.org/10.1016/j.optlastec.2022.107846.

[13] G.E. Bean, D.B. Witkin, T.D. McLouth, D.N. Patel, R.J. Zaldivar, Effect of laser focus shift on surface quality and density of Inconel 718 parts produced via selective laser melting, Addit. Manuf. 22 (2018) 207–215, https://doi.org/10.1016/j.addma.2018.04.024.

[14] R.A. Rahman Rashid, H. Ali, S. Palanisamy, S.H. Masood, Effect of process parameters on the surface characteristics of AlSi12 samples made via Selective Laser Melting, Mater. Today Proc. 4 (2017) 8724–8730, https://doi.org/10.1016/j.matpr.2017.07.221.

[15] A. Koglbauer, More than beam profiling: a new approach for beam diagnostics in 3D additive manufacturing systems, Laser Tech. J. 15 (2018) 40–44, https://doi.org/10.1002/latj.201800016.

[16] R. Aman, A. Krishnan, A. Dhakad, J. Hay, Novel pin-hole analyzer for characterizing laser beam quality across the build environment in L-PBF, ASPE-euspen 2022 Summer Topical Meeting: Advancing Precision in Additive Manufacturing (2022) 186–187.

[17] F.M. Haran, D.P. Hand, C. Peters, J.D.C. Jones, Focus control system for laser welding, Appl. Opt. 36 (1997) 5246, https://doi.org/10.1364/AO.36.005246.

[18] D.P. Hand, M.D.T. Fox, F.M. Haran, C. Peters, S.A. Morgan, M.A. McLean, W. M. Steen, J.D.C. Jones, Optical focus control system for laser welding and direct casting, Opt. Lasers Eng. 34 (2000) 415–427, https://doi.org/10.1016/S0143-8166(00)00084-1.

[19] P.J. DePond, J.C. Fuller, S.A. Khairallah, J.R. Angus, G. Guss, M.J. Matthews, A. A. Martin, Laser-metal interaction dynamics during additive manufacturing resolved by detection of thermally-induced electron emission, Commun. Mater. 1 (2020) 92, https://doi.org/10.1038/s43246-020-00094-y.

[20] J.C. Lagarias, J.A. Reeds, M.H. Wright, P.E. Wright, Convergence properties of the Nelder–Mead simplex method in low dimensions, SIAM J. Optim. 9 (1998) 112–147, https://doi.org/10.1137/S1052623496303470.

[21] P.E. Verboven, Distortion correction formulas for pre-objective dual galvanometer laser scanning, Appl. Opt. 27 (1988) 4172–4173, https://doi.org/10.1364/AO.27.004172.

[22] J. Berez, L. Sheridan, C. Saldaña, Extreme variation in fatigue: fatigue life prediction and dependence on build volume location in laser powder bed fusion of 17-4 stainless steel, Int. J. Fatigue 158 (2022) 106737, https://doi.org/10.1016/j.ijfatigue.2022.106737.

[23] T.P. Moran, D.H. Warner, A. Soltani-Tehrani, N. Shamsaei, N. Phan, Spatial inhomogeneity of build defects across the build plate in laser powder bed fusion, Addit. Manuf. 47 (2021) 102333, https://doi.org/10.1016/j.addma.2021.102333.